Int. J. Electrochem. Sci., 8 **(2013)** 12837 - 12850

International Journal of
ELECTROCHEMICAL
SCIENCE
www.electrochemsci.org

Effect of Electrochemical Factors on Formation and Reduction of Silver Oxides

Ye Wan[1,2,3,*], *Xianle Wang*[2], *Siyu Liu*[2], *Yanbo Li*[1], *Hong Sun*[2], *Qing Wang*[1]

[1] School of Materials Science and Engineering, Shenyang Jianzhu University, Shenyang 110168, China
[2] School of Traffic and Mechanical Engineering, Shenyang Jianzhu University, Shenyang 110168, China
[3] State Key Laboratory for Corrosion and Protection, Institute of Metal Research, Chinese Academy of Sciences, Shenyang, 110016, China
[*]E-mail: ywan@sjzu.edu.cn

Received: 4 August 2013 / *Accepted:* 6 September 2013 / *Published:* 20 October 2013

Polarization of silver in NaOH solution with various electrochemical parameters was investigated by cyclic voltammetry and scanning electron microscope. The resulting cyclic voltammograms reveal that the observed midpoint potential and current density of the peaks during the anodic scan and the reversed scan can be shifted significantly depending on scan rate and NaOH concentration. The shapes of the peaks in the first cycle were different from the other cycles of silver' cyclic voltammetry. The peaks were barely dependent of scan rate since the second cycle. Two layers of Ag_2O, which owed to the formation of dual anodic peaks of Ag_2O, appeared during the anodic scan of silver' cyclic voltammetry. Two secondary anodic peaks were formed if the scan rate was no less than 20 mV/s and NaOH concentration was no less than 0.5 $mol{\cdot}L^{-1}$ The trenched images by focus ion beam system explored that the depth of the polarized silver was approximately 810 *nm* after three cycles with a scan rate of 10 *mV/s* in 1 $mol{\cdot}L^{-1}$ NaOH solution. The images of the polarized silver clarified the formation and shifts of the peaks in silver's cyclic voltammetry.

Keywords: Silver; Cyclic voltammetry; Anodic peak; Reduction peak; Focus ion beam

1. INTRODUCTION

Silver oxide was often used as a cathodic electrode, coupled with other anodes, in rechargeable power sources for high energy/power applications due to its performance, safety, reliability, and high specific energy/energy density [1], such as silver oxide-zinc, silver oxide-aluminum, and silver oxide-lithium batteries in alkaline solution. Therefore, the successive stages of electrolytic formation and

reduction of silver oxides have attracted much attention [2-13] on account of the interest in oxides of silver as a cathode material in primary and specialized secondary batteries.

Up to now many mechanisms concerning formation and reduction of silver oxides in alkaline solution have been proposed, such as diffusion control mechanism [2], dissolution mechanism [14-15], preferential oxidation of active sites [16], autocatalytic mechanism [7] and nucleation and propagation rate controlling mechanism [2, 17-18]. All those mechanisms look reasonable. However, no direct evidence could be used to prove the exact mechanism of formation and reduction of silver in alkaline solution at the time.

The present paper used cyclic voltammetry, combined with Focus Ion Beam (dual beam) to examine and assess the effects of a wide range of electrochemical parameters on formation and reduction of silver oxides in NaOH solution and most of important, provide a clear evidence for nucleation and propagation rate controlling mechanism.

2. EXPERIMENT

Sample.− Silver samples (99.99% purity) with the size of 10 *mm* × 10 *mm* × 1.5 *mm* were polished with SiC paper (successively 800 and 1000 grits), degreased with alcohol and rinsed with deionized (DI) water, dried and kept in desiccators with silica gel for at least 24 hours. High purity water (Millipore > 20 $M\Omega\,cm$) was used throughout.

Electrochemical methods.− A conventional three electrode cell was used for electrochemical studies. The cell exposed a 1 cm^2 portion of the samples to be work electrodes. There was a small hole in every sample. A silver lead connected to the sample through the hole was contacted with the cell cable of the electrochemistry instrument. The counter electrode is a flat platinum mesh. All the potentials were measured against an Hg/Hg_2Cl_2/saturated KCl reference electrode (SCE). The electrochemical experiments with low scan rate (≤ 20 *mV/s*) were conducted with an electrochemical instrument (LK3200A, Lanlike Co. Ltd., Tianjin, CN) combined with an electrochemistry software named LK3200A®. The potential range of CV with LK 3200A was chosen between -0.5 V_{SCE} (*V* vs SCE) and 1.0 V_{SCE} (*V* vs SCE). The electrochemical experiments with higher scan rate (> 20 *mV/s*) were conducted with potentiostat (PARSTAT 2273, Princeton Applied Research, AMETEK, USA) combined with an electrochemistry software named Electrochemistry PowerSuite®. The potential range of CV with Parstat 2273 was chosen between -0.5 V_{SCE} (*V* vs SCE) and 1.0 V_{SCE} (*V* vs SCE). The electrolyte for cyclic voltammetry (CV) was sodium hydroxide (NaOH) with various concentrations. It was delayed 20 seconds in NaOH solution before every CV scan. NaOH solutions were made from Sinopharm certified NaOH and DI water. Each electrochemical experiment was repeated at least three times on different occasions and the variation in response was less than 5 mV at 25 ºC.

Surface examination.− The morphologies of the samples were observed using scanning electron microscopy (SEM) (Nova NanoSEM 430, FEI, Netherland). A dual beam focus ion beam (FIB) (Helios nanolab 650, FEI, Netherland) system uses gallium ions to mill a region of interest with nanometer scale precision and examine the cross-section images of the samples. Imaging was

performed with an accelerating voltage of 15.0 KV by Nova NanoSEM 430 and 10.0 kV by Helios nanolab 650 to produce high resolution images.

3. RESULT

3.1 CVs of silver at different cycles

Fig.1 presents the cyclic voltammograms ($I/A{\cdot}cm^{-2}$ vs E) of silver with a scan rate of 5 *mV/s* in 0.5 $mol{\cdot}L^{-1}$ NaOH solution. There were two main oxidation peaks (pa1 and pa2) during the anodic scan and two reduction peaks (pc3 and pc4) during the reversed scan in every cycle of the CV curves. For example, in the first cycle of silver of Fig.1, the first oxidation peak 'pa1' observed at about 0.268 V_{SCE} (V vs SCE) and the second oxidation peak 'pa2' was observed at about 0.573 V_{SCE} during the anodic scan, which was accompanied by the appearance of the two reduction peaks during the reversed scan at about -0.03 V_{SCE} and 0.274 V_{SCE} to the two oxidation peaks respectively. The peaks 'pa1' and 'pa2' corresponded to the formation of Ag_2O and AgO in NaOH solution respectively and the peaks 'pc4' and 'pc3' during the reversed scan corresponded to the reduction of AgO→ Ag_2O and Ag_2O→Ag respectively [2-3,18,20-23].

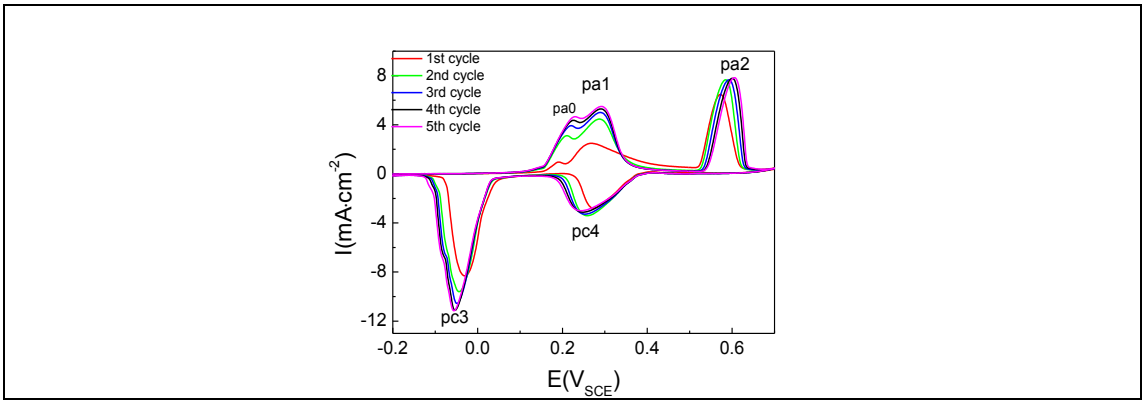

Figure 1. Cyclic voltammograms of Ag with five cycles in 0.5 $mol{\cdot}L^{-1}$ NaOH with a scan rate of 5 *mV/s*.

Fig. 2(a) shows the midpoint potentials (E_{mid}) and the corresponding current density (I_{mid}) of the peaks in Fig.1. The changes of peak characteristic from the first cycle to the second cycle were the biggest through the five cycles. Compared the first cycle, every oxidation peak (pa1 or pa2) shifted to a more positive potential during the anodic scan and every reduction peak (pc1 or pc2) to more negative potential during the cathodic scan in the following four cycles of silver's CVs. However, silver's CVs show the positions of peaks were almost stable at different circles and didn't change much with increasing cycling through the second cycle to the fifth cycles. For every peak in the five cycles of the CV curves, the midpoint current densities of the peaks didn't increase much with increasing cycling except the first cycle. For example, the values of I_{pa1} at different cycles were almost

the same through the second to the fifth cycles, but I_{pa1} increased from 2.49081 *mA/cm*^{2} of the first cycle to 5.4899 *mA/cm*^{2} of the fifth cycle, which is more than two times of I_{pa1} of the first cycle.

The potential of the pre-peak 'pa0', is a little negative to the potential of the peak 'pa1' and appeared in the anodic scan of every cycle in silver's CVs. The shapes of the peak 'pa0' didn't change much but the peak shifted to a little more positive potentials during the anodic scan with the increasing cycling except the first cycle. Continuous cycling from the second cycle produced small changes in pre-peak height which accompanied by similar changes in the height of the Ag_2O peak. The ratio of Ipa1 to Ipa0 was shown in Fig. 2(b). It can be seen that the ratio decreased with increasing cycling in the first two cycles and it changed little with continuous cycling since the third cycle, seen in Fig.2 (b).

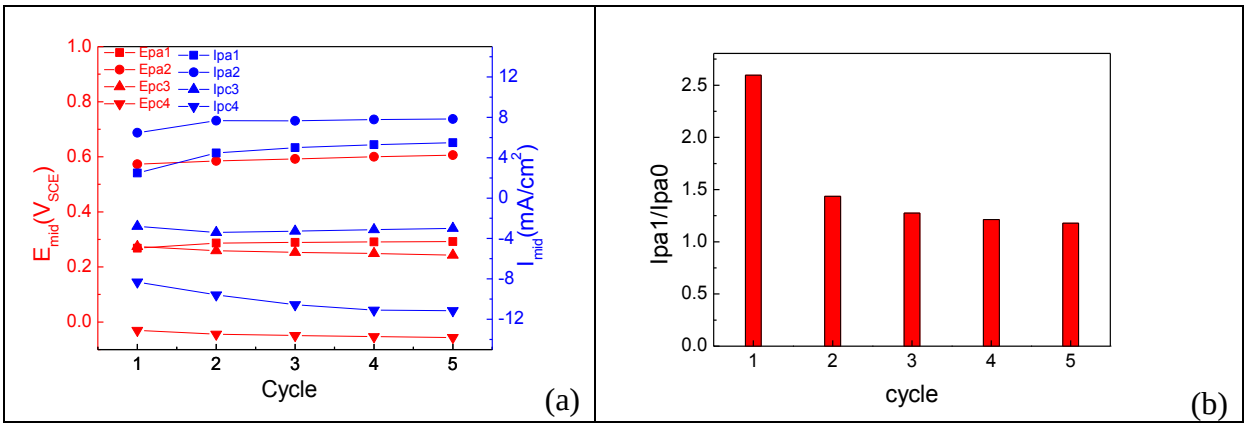

Figure 2. (a) Peak characteristic of the curves and (b) ratio of Ipa1 to Ipa0 in Fig.1.

3.2 CVs of silver at different scan rates

It was recorded in the first cycle of silver's CVs in 0.5 *mol·L*$^{-1}$ NaOH that there was one secondary anodic peak 'paA1' when the scan rate was 10 *mV/s* and two secondary anodic peaks 'paA0' and 'paA1' when the scan rate was 20 *mV/s* during the reversed scan (cathodic scan), seen in Fig.3(a) and Fig.3(b).

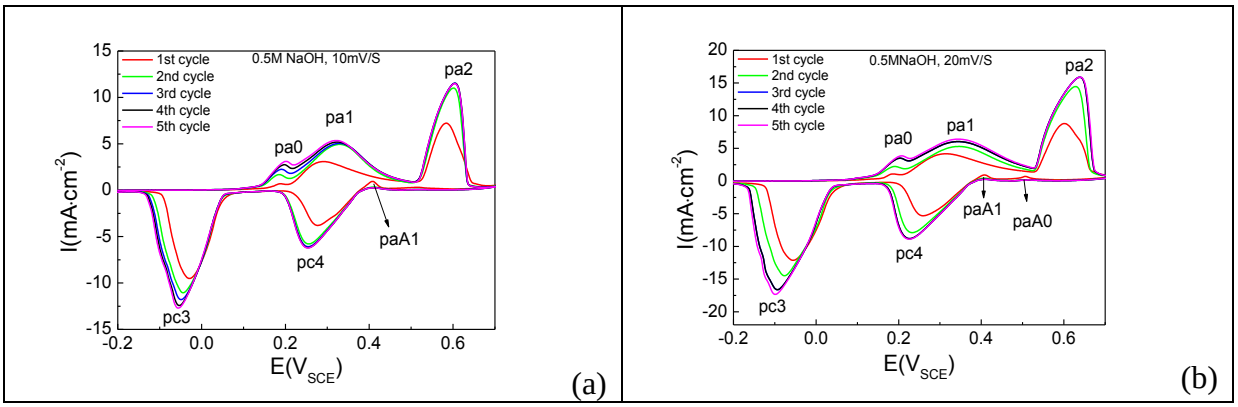

Figure 3. Cyclic voltammograms of Ag in 0.5 *mol·L*$^{-1}$ NaOH solution with scan rates of 10 *mV/s* (a) and 20 *mV/s* (b).

The secondary anodic peaks were found to be scan rate dependent and disappeared after the first cycle. The bigger the scan rate was, the bigger I_{paA1}/I_{pa2} was. It is interesting to note that no secondary anodic peak was detected if the scan rate was no more than 5 *mV/s* and in 0.5 *mol·L*$^{-1}$ NaOH, just as in Fig.1.

CVs were run repeatedly five cycles for silver at various scan rates over the range from 1 *mV/s* to 20 *mV/s* in 0.5 *mol·L*$^{-1}$ NaOH. Since the shapes of the oxidation peaks and reduction peaks in silver's CV didn't change much with increasing cycling except the first cycle, the different CV curves and the corresponding peak characteristic of the second cycle (arbitrary chosen) were plotted as a function of the scan rate in Fig.4. Fig.4(b) and Fig.4(c) are plots of E_{mid} and I_{mid} *vs* scan rate for silver's CVs in 0.5 *mol·L*$^{-1}$ NaOH respectively. Every oxidation peak shifted to more positive potentials and every reduction peak shifted to more negative potentials in Fig.4 (a). Every peak, either the oxidation peaks or reduction peaks, became broader with increasing scan rate. On the other hand Peak pa2 became sharper and higher with respect to Peak pa1. Compare to Peak pa1 with various scan rates, the pa1 peak was the broadest and the pa2 peak was the highest when the scan rate was 20 *mV/s*.

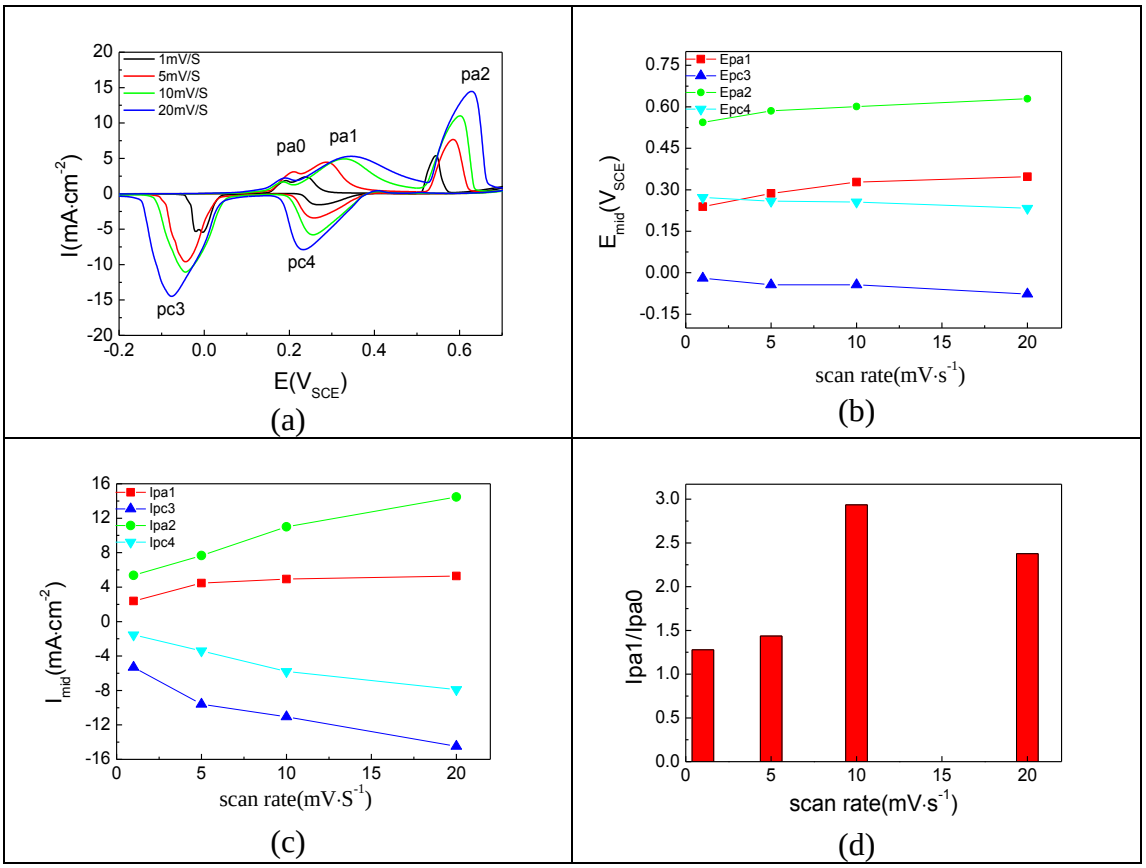

Figure 4. (a) Cyclic voltammograms of Ag with various scan rate in 0.5 *mol·L*$^{-1}$ NaOH solution, (b) peak potential of the curves in Fig.4(a), (c) peak current density of the curves in Fig.4(a), (d) ratio of Ipa1 to Ipa0 in Fig.4(a).

From Fig. 4(c), it can be seen that every peak current density, for both of oxidation peaks and reduction peaks in silver's CV in 0.5 *mol·L*$^{-1}$ NaOH, increased with scan rate. However, the current

density of Peak pa2 increased faster than the other peaks with scan rate. The changes of peak potential and peak current density indicated the observed peak characteristic was dependent of scan rate over the range 1-20 *mV/s*. Fig.4(d) shows the ratio of Ipa1 to Ipa0 in Fig.4(a), it seems the ratio increased with scan rate when it was no more than 10 *mV/s*, and decreased with scan rate when it was bigger than 10 *mV/s*.

3.3 CVs of silver in NaOH solutions with different concentration

Fig.5 presents the first cycle of silver's CV in NaOH solution with various concentrations at a scan rate of 25 *mV/s*. It can be seen from Fig.5 that the peak became sharper with increasing NaOH concentration. Fig.6 illustrates E_{mid} of the peaks and I_{mid} of silver's CVs in Fig.5. Both of E_{mid} and I_{mid} varied with NaOH concentration. The midpoint oxidation potentials of the peaks shifted more negative and the midpoint reduction potentials of the peaks shifted more positive with increasing NaOH concentration. E_{mid} of pa1 obtained in 1 $mol{\cdot}L^{-1}$ NaOH was 81 mV more negative than that observed in 0.5 $mol{\cdot}L^{-1}$ NaOH. It looks I_{mid} of every peak increased linearly with NaOH concentration. I_{mid} of pa1 in 1 $mol{\cdot}L^{-1}$ NaOH was more than 7 times bigger than that in 0.1 $mol{\cdot}L^{-1}$ NaOH.

Fig.5 shows the secondary anodic peak 'paA1' appeared in 0.5 $mol{\cdot}L^{-1}$ as well as in 1 $mol{\cdot}L^{-1}$ NaOH. but no secondary anodic peak was detected in 0.1 $mol{\cdot}L^{-1}$ NaOH when the scan rate was 25 *mV/s*. A very small secondary anodic peak 'paA0' was also recorded for silver's CV in 1 $mol{\cdot}L^{-1}$ NaOH . Compared the CV curves of Fig.3 and Fig.5 in the case of 0.5 $mol{\cdot}L^{-1}$ NaOH, I_{paA1}/I_{pa2} in Fig.3 was bigger than in Fig.5 even though the scan rate in Fig.3 was smaller than in Fig.5. As the data of Fig.3 was performed in LK3200A, while the data of Fig.5 in PARSTAT 2273. The results indicated the secondary anodic peak was dependent of the sensitivity of electrochemical instrument.

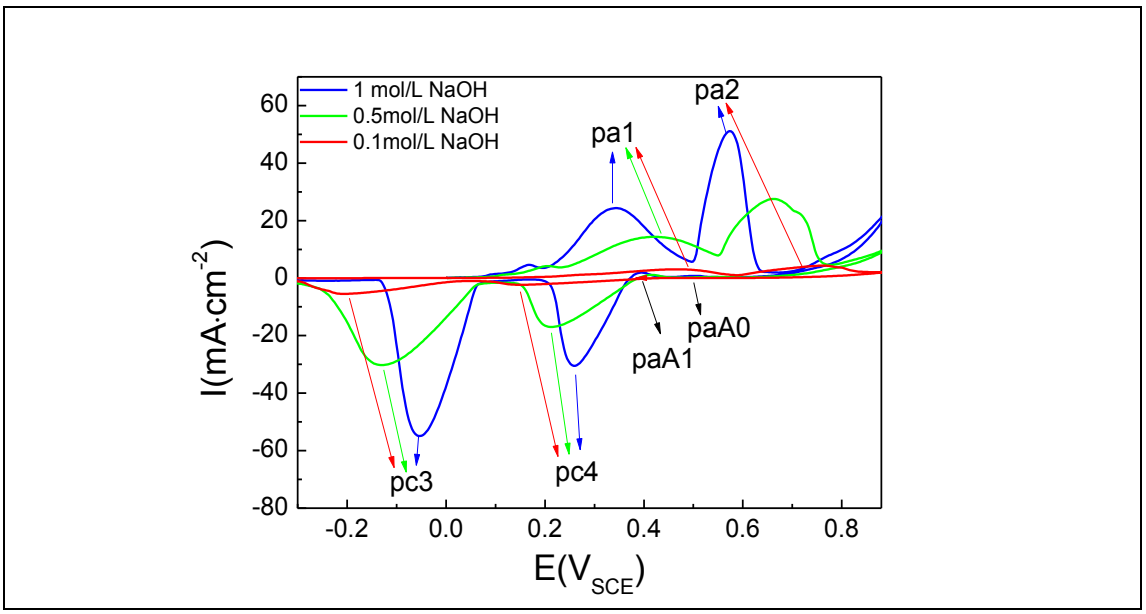

Figure 5. Cyclic voltammograms of silver in NaOH solution with different concentration at a scan rate of 25 *mV/s*.

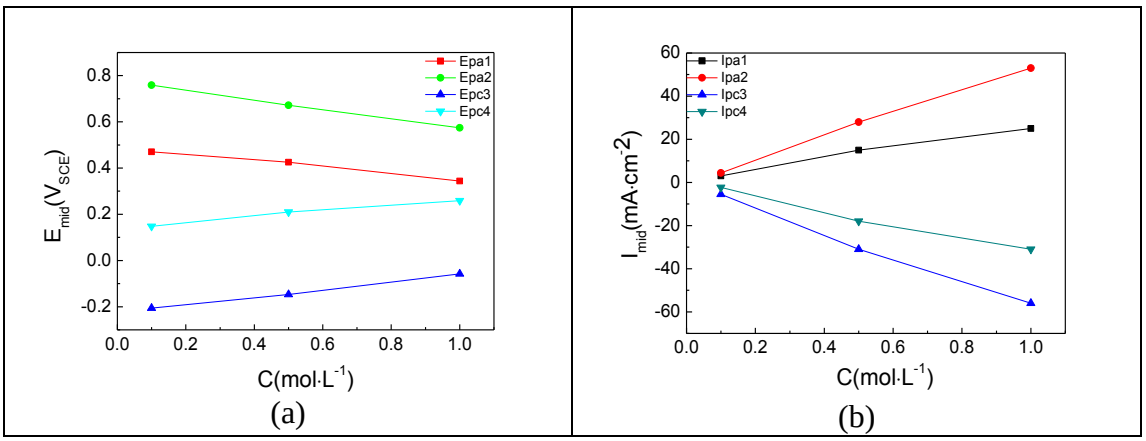

Figure 6. (a) Relationship of E_{mid} and concentration of NaOH solution in Fig.5, (b) relationship of I_{mid} and concentration of NaOH solution in Fig.5.

3.4 SEM morphology

Fig.7 presents SEM images of silver very shortly after different peaks in the third cycle of silver's CV with a scan rate of 10 *mV/s* in 1 *mol·L*$^{-1}$ NaOH solution. Fig.7 (a) show two layers of Ag_2O formed promptly after the first peak (pa1). This figure provides a clear evidence for Briggs's work [19] that the existence of two types of layers Ag_2O. It is clear that Ag_2O crystals with the size ranging from 100 *nm* to 285 *nm* were formed on the outer oxidation layer of silver. Many pores were left in the outer layer, which was next to the solution. Ag_2O nano crystals with the size of approximately 20 *nm* agglomerated together to form the inner layer. Some agglomerated and developed upward and made many clusters of nano crystals scattered in the holes of the outer layer.

Fig.7(c) and (d) are SEM images of silver promptly after the second peak (pa2) in the third cycle of silver's CV. It can be seen form Fig.7(c) that AgO nucleated and developed from Ag_2O and following the contour of Ag_2O crystals during the continuous scanning of CV after the first peak. The reactions taking place initially during the process from Ag_2O to AgO occurred at the outer layer of the polarized silver. AgO centres nucleated on the Ag_2O layer and progressively covered outer layer with increasing time. This figure indicated that the growth of larger crystals was at the expense of small ones. Many new formed AgO crystals coalesced with each other and encased the oxidation layers of silver, seen in Fig.7 (d). This phenomenon is assessed the suggestion of Fleischmann [17] that the reaction of $Ag_2\rightarrow$ AgO initiated at outer surface of the electrode.

During the reversed scan, silver oxides were reduced. Fig.7 (e) and (f) are SEM images of silver immediately after the third peak (pc4) in the third cycle of silver's CV. The images show the reaction of AgO→Ag_2O occurred simultaneously in the outer and the inner oxidation layers at this stage. Many cracks appeared in the reduction scan on the surface. Ag_2O crystals with the size ranging from 100 *nm* to 250 *nm* were covered on the surface of silver. Plenty of crystals agglomerated to form the crystals more than 400 *nm* in size, seen in Fig.7 (e). Shortly after the fourth peak (pc3), silver crystals were reduced from Ag_2O and followed the profile of Ag_2O, seen in Fig.7 (g) and (h). The sizes of silver crystal are smaller than that of Ag_2O. Many cracks and holes are left on the surface of

silver. Fig.8 is the 52º-tilted SEM images of the same sample as in Fig.7 (g) and (h). Fig.8 (a) shows the size of silver crystal was about 200 *nm* ~ 500*nm*. In order to know the cross-section protocol of the polarized silver during the CV cycling, FIB system was used to trench the desired surface of silver, seen in Fig. 8 (b).

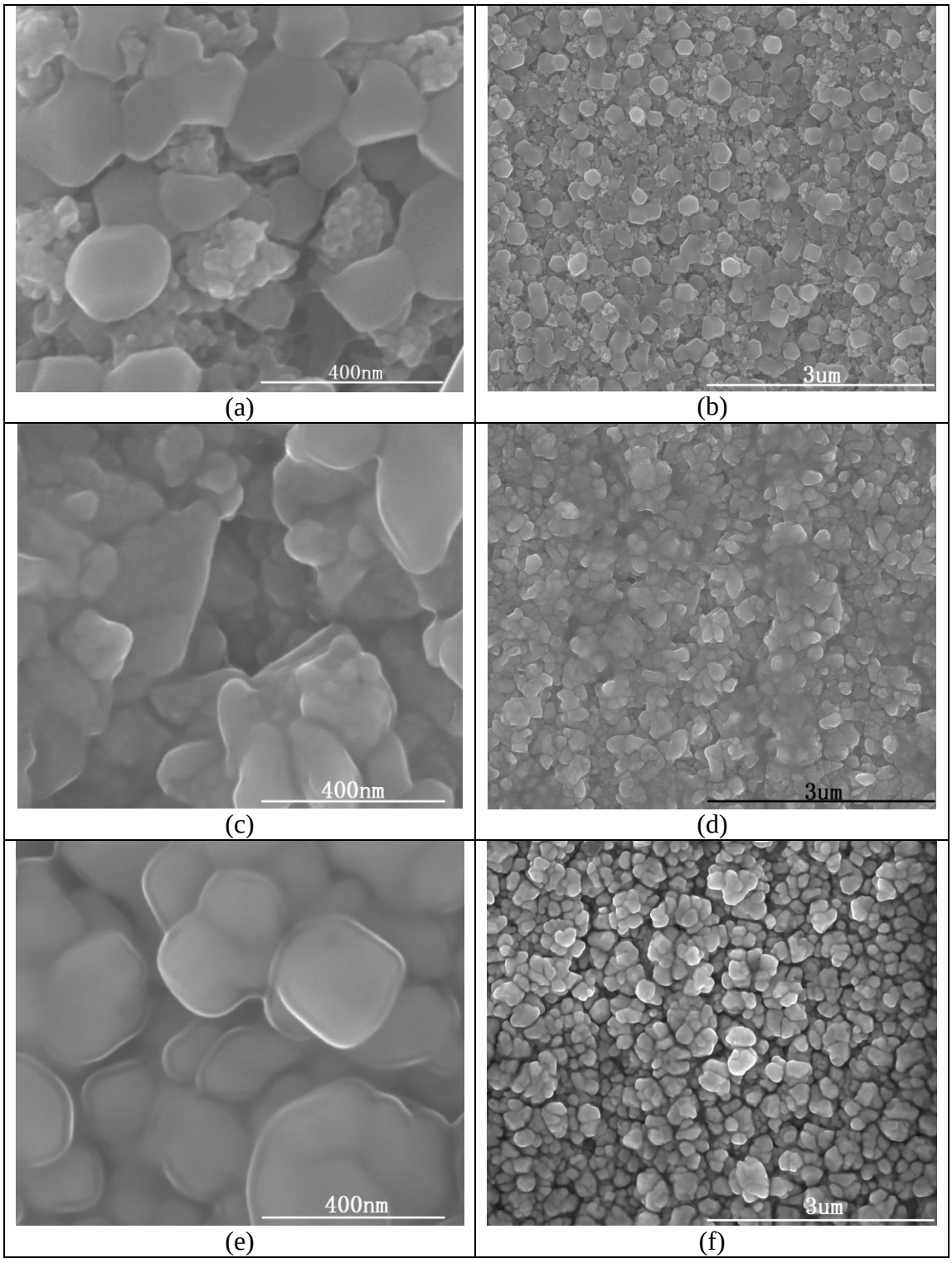

(a) (b)

(c) (d)

(e) (f)

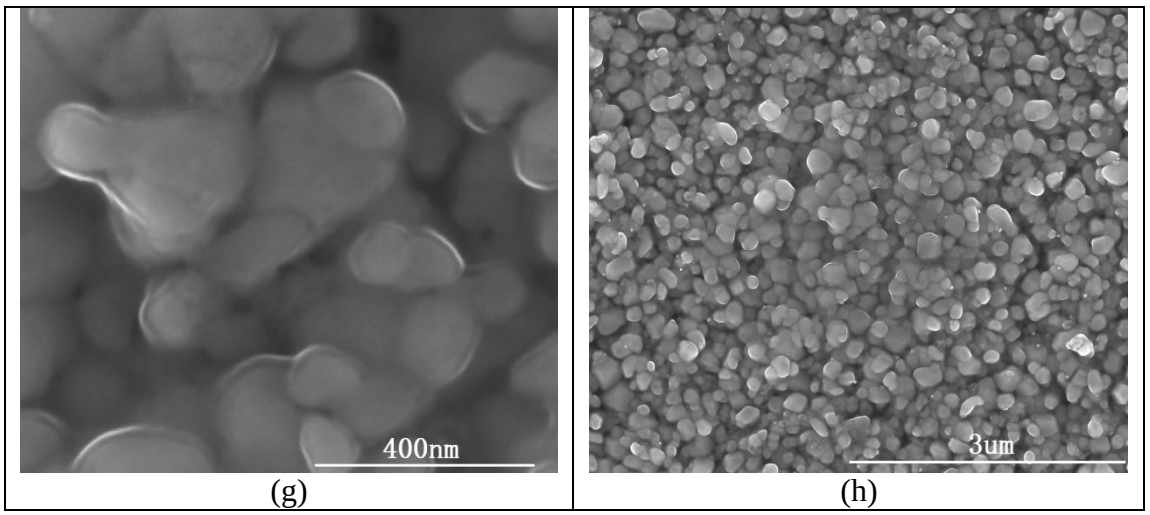

Figure 7. High- and low-magnification SEM images of silver shortly after different peaks of CV with a scan rate of 10 *mV/s* in 1 $mol \cdot L^{-1}$ NaOH solution, (a) and (b) oxidation peak 'pa1', (c) and (d) oxidation peak 'pa2', (e) and (f) reduction peak 'pc4', (g) and (h) reduction peak 'pc3'.

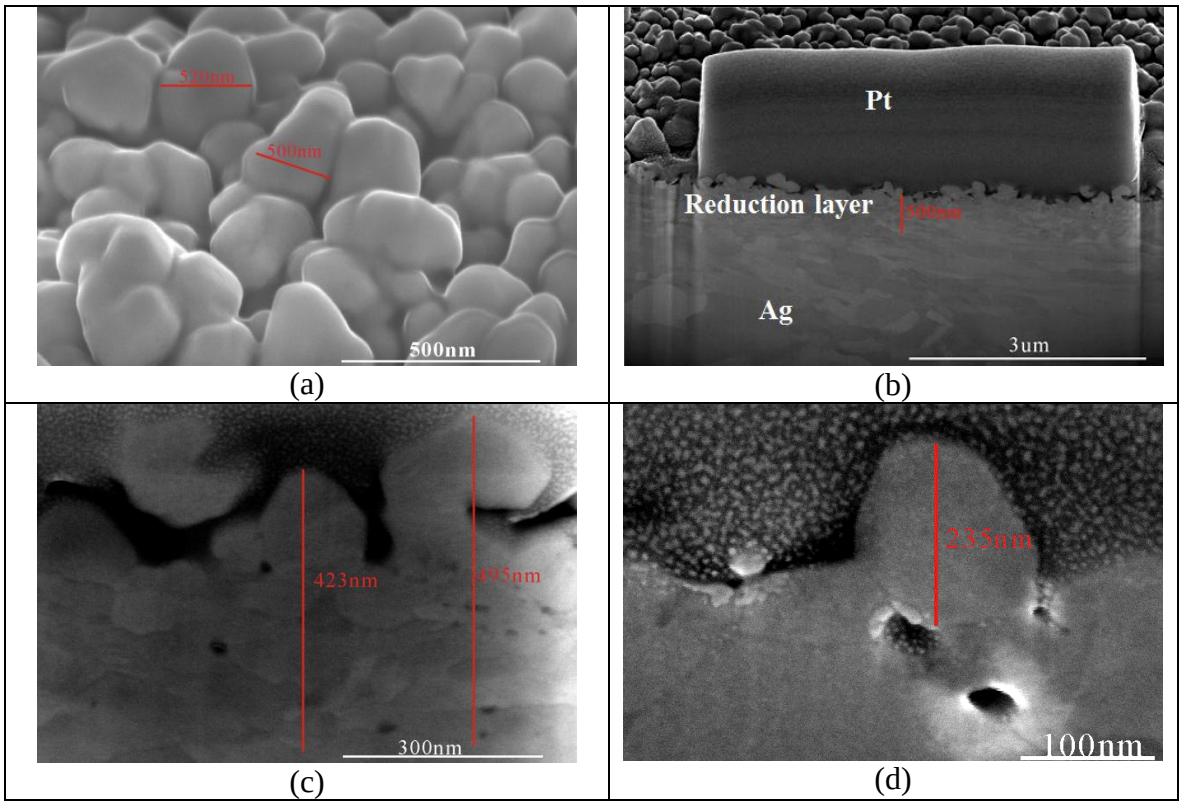

Figure 8. 52º-titled SEM images of the same sample as in Fig.7 (g) and (h). (a) surface image, (b) image of the trenching area, (c) cross-section image (250,000×), (d) cross-section image (500,000×).

Pt was deposited on the surface of silver in the sample chamber of FIB system just before trenching to protect the layer from ion beam. Fig. 8(c) and (d) are the cross-section images part of Fig.

8(b). Fig. 8(b) and (c) illuminate that the polarized layer of silver were about 812 *nm* (500 *nm*/cos52º) after three cycles. Fig. 8(c) shows that cracks and holes were formed in the polarized layer of silver. The image enlarged 500,000×, Fig.8(d), shows the deposited Pt appeared in the holes inside of the polarized layer. This figure provides an undoubted evidence that the holes pierced through the polarized layer's interior from silver's outmost surface, which was next to NaOH solution during the continuous cycling of CV.

Fig.9 shows SEM images of silver after five cycles' CV in 0.5 $mol \cdot L^{-1}$ NaOH solution with various scan rates. The surfaces of all silver samples were covered with Ag crystals with various sizes. At a scan rate of 1 *mV/s*, silver nucleated from Ag_2O and propagated into crystals with the size of about 30 *nm*. Since the scan rate is slow, the reaction of $Ag_2O \rightarrow Ag$ was controlled by diffusion of reagent in the Ag_2O layer. The reduced silver had time to agglomerate together and form larger clusters (about 300 *nm* ~ 500 *nm*). Plenty of holes were heaped because the accumulated clusters have large surface area.

As the scan rate increased, the current density of the peak 'pc3' increased, which made the propagation of silver crystals increased. Therefore, the size of crystal increased with scan rate, seen from Fig.9 (a), (c), (e) and (g). When the scan rate was *20 mV/s*, large numbers of silver nuclei were formed instantaneously at Ag_2O/electrolyte interface.

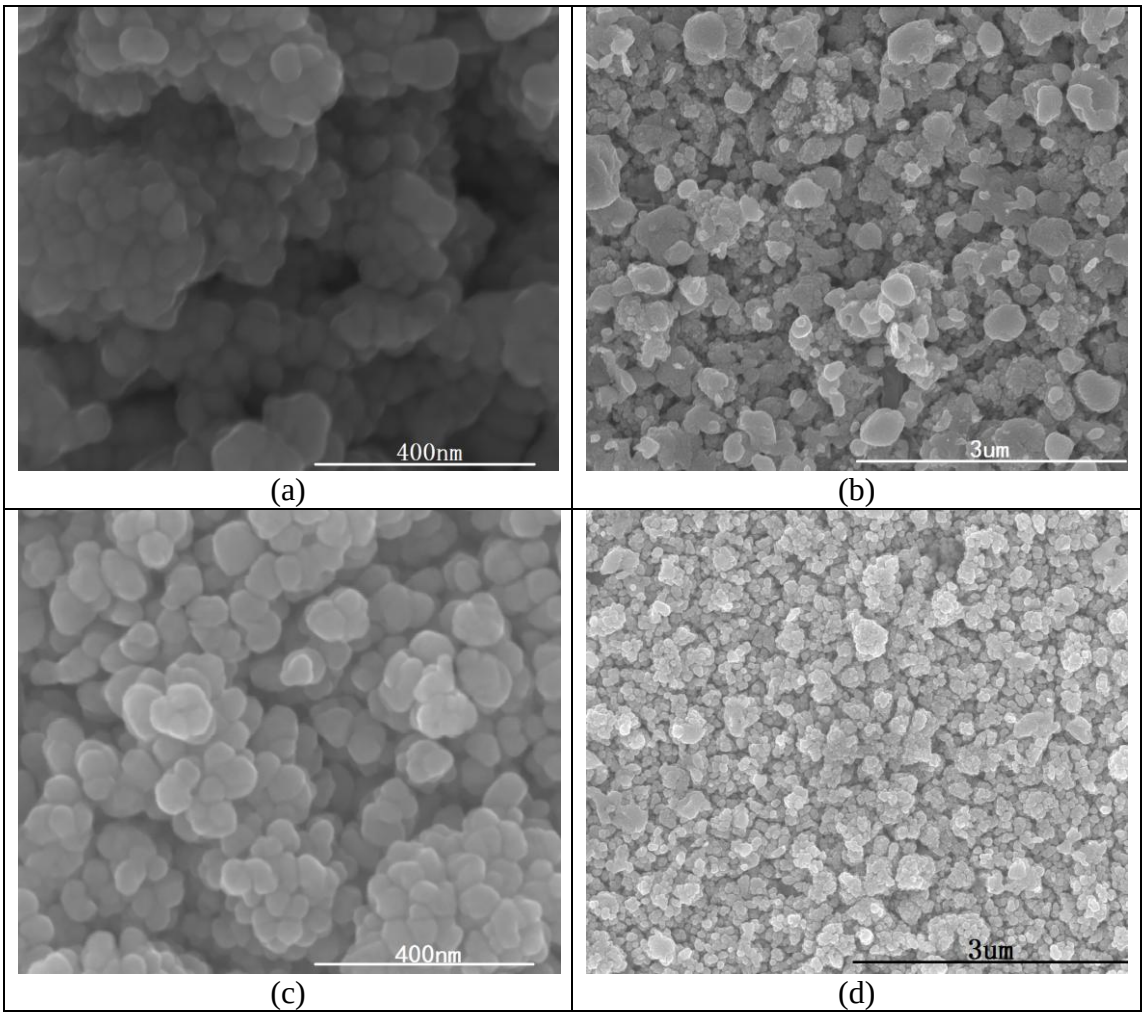

(a) (b)

(c) (d)

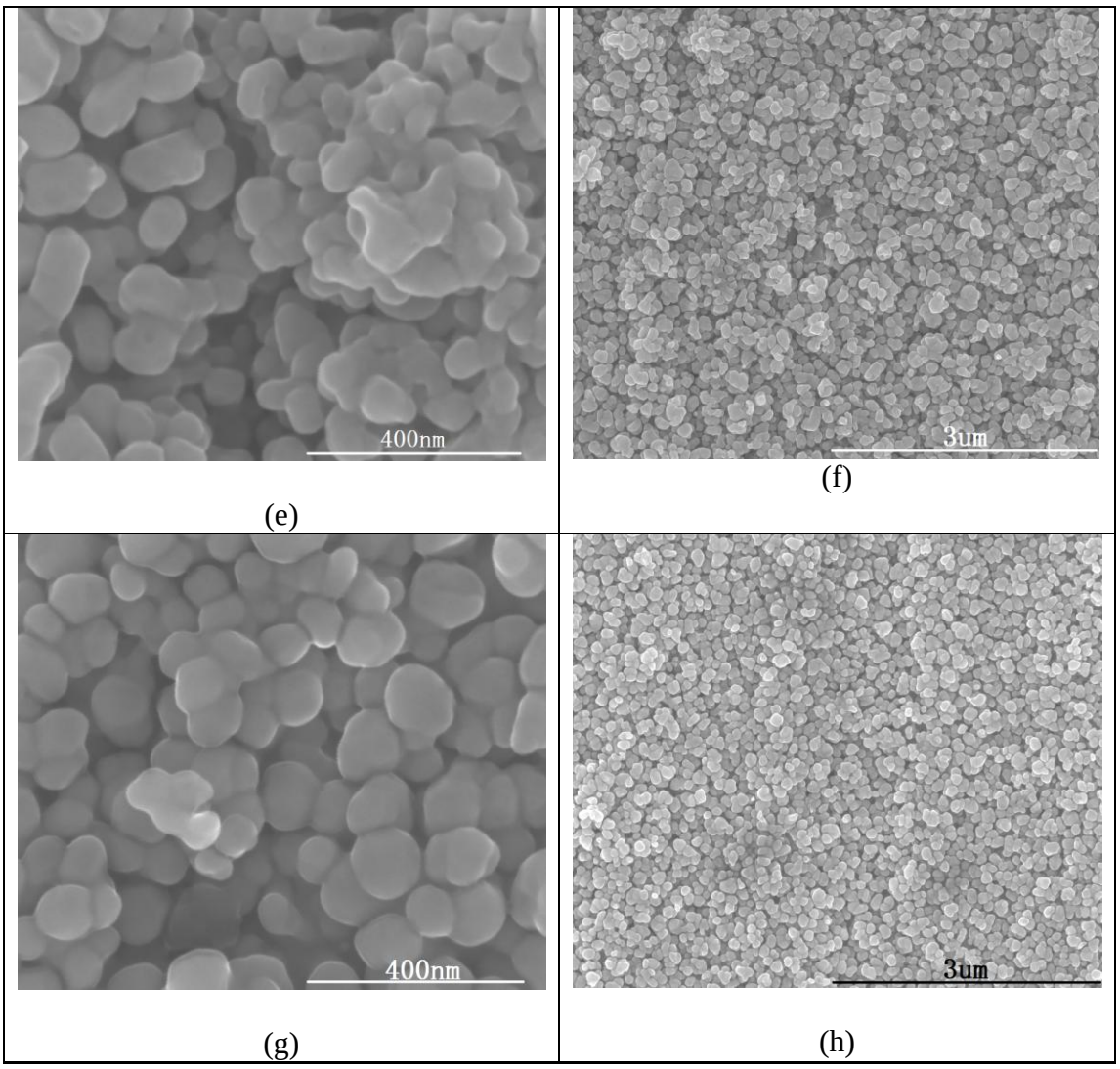

Figure 9. High- and low-magnification SEM images of the reduced silver's surfaces after five cycles' CV in 0.5 $mol{\cdot}L^{-1}$ NaOH solution with various scan rates, (a) and (b) 1 *mV/s*, (c) and (d) 5 *mV/s*, (e) and (f) 10 *mV/s*, (g) and (h) 20 *mV/s*.

The size of reduced silver crystal was about 100 *nm* (Fig.9 (g)), and silver crystals didn't have so much time to aggregate as at lower scan rate. This might be the reason why the silver crystals reduced with higher scan rate was more uniform in size and distribution than with lower scan rate (seen in Fig.9 (b), (d), (f) and (h)), which may also be attributed to the more rapid and uniform rate of nucleation for experiments [19].

4. DISCUSSION

Three peaks appeared during the anodic scan in silver's CVs. One is so-called pre-peak (Peak pa0) [3-4] and the others are normal anodic peaks (Peak pa1 and Peak pa2). Peaks 'pa1' and 'pa2' in Fig. 1 were in agreement with the findings from other workers [2-3,18,20-23] that appearance of anodic peaks corresponded to the formation of Ag_2O and AgO in NaOH solution respectively. Peaks

'pc4' and 'pc3' during the reversed scan corresponded to the reduction of AgO→ Ag_2O and Ag_2O→Ag respectively.

Generally, the reversibility of electrochemical reaction is determined by the redox peak potentials on the scan rate. The peak potentials are not dependent on the scan rate in the reversible process, but are dependent in the irreversible process. The shift of reduction peak to the negative potential and of the oxidation peak to positive potential with increasing scan rate in Fig.4 indicates that this redox process is irreversible [24-26]. On the other hand, according to the criterion for the mechanism of reversible reaction potential [27], if the difference in cathodic (E_{pc}) and anodic (E_{pa}) peak potentials is around $60/n\ (mV)$, the reaction is reversible electron transfer process. Here, n is valency of ion and $n = 1$ because it is two-step one-electron transfer process in the reaction of AgO→Ag_2O →Ag and Ag_2O.

For the peaks (pa1 and pc3) in the first cycle of the silver's CV curves with a scan rate of 5 *mV/s*, $\Delta E_p(Ag_2O) = E_{pa1} - E_{pc3} = 0.268 - (-0.03) = 0.298\ V > 56.5mV$, and $\Delta E_p(AgO) = E_{pa2} - E_{pc4} = 0.573 - 0.274 = 0.299\ V > 56.5mV$. $\Delta E_p(Ag_2O)$ is the potential difference of oxidation and reduction of Ag_2O, and $\Delta E_p(AgO)$ is the potential difference of oxidation and reduction of AgO in the CV curves. For the fifth cycle, $\Delta E_p(Ag_2O) = 0.348\ V$, and $\Delta E_p(AgO) = 0.363\ V$. All the values of the ΔE_p in silver's CVs were more than 60 *mV*. These results are indicative of an irreversible one- electron transfer.

Fig. 5 and Fig.6 show midpoint oxidation potentials of the peaks shifted more negative and the midpoint reduction potentials of the peaks shifted more positive with increasing NaOH concentration. The peak separation owing to the shifts remained constant at 50-60 mV expected for a mixture of finite and infinite diffusion during the polarization [28].

Current density depended on the concentration gradient of reagents in the diffusion layer, and the concentration gradient decreased with increasing time. Therefore, the bigger the scan rate was, the bigger the current densities of the peaks were.

Changes of current in silver' CVs after the first cycle might be attributed to the increase of surface roughness. After formation and reduction of silver oxides, the geometrical surface of silver surface became rougher than the polished silver. This might be the reason that the shapes of the peaks in the first cycle were greatly different from the other four cycles, seen in Fig.1 and Fig.3. Silver having rougher surface has lower work function [29], which decreased the corrosion potential of silver and made its current density higher than the smoother one in the first cycle. Grozdić et al. [22] also reported that the real surface of an electrode arises increasing after several charge-discharge cycles. A real surface of an electrode after seven cycles was found increased for three times and further cycling has no influence to the electrode surface. The results in Fig.1 indicated surface roughness changed much after 1 cycle and barely changed since the second cycle.

There was Peak 'pa0' in all of silver's CVs. The peak in the first cycle was different from the other cycles. Amberose et al. [4] and Giles et al. [14] also reported the formation of the peak in the oxidation of silver and proposed the peak was coming from the a soluble species $Ag(OH)_2^-$ diffusing away from the electrode. The two peaks 'pa0' and 'pa1' in the second cycle through the fifth cycles might be the consequence of the formation of the two layers of Ag_2O in Fig.1. Monolayer Ag_2O was formed at preferred sites of the basal silver. This monolayer progressively blocked off the dissolution

reaction. Droog et al. [2] proposed that oxidation of Ag to Ag_2O is a diffusion-controlled reaction and the diffusion control was established in the solid phase. Fleischmann et al. [17] suggested that the basal layer determined the growth kinetic of Ag_2O. At still higher potentials the current rose again due to the thickening of the monolayer and formation of a dual Ag_2O layer structure [14]. From the surface image in Fig.8, it can be deduced there are many pores in the inner layer of the polarized silver, and electrolyte can penetrated into basal layer of silver. Therefore, the peak 'pa0' will appear at the next cycling.

When the scan rate was big enough, two secondary anodic peaks appeared in the first cycle of silver's CVs, seen in Fig. 3(b). Many researchers have found the secondary anodic peak 'paA0' in the cathodic scan of silver's CV [3,7,15,17] and regarded this peak was arisen from an anodic reaction during the cathodic scan and was owing to the autocatalytic generation of AgO. According to the potential positions of the two peaks, which were believed to be attributed to the formation of a layer Ag_2O and the autocatalytic effect of AgO. The roughness of the surface of polarized silver changed much after the first cycle of silver's CV. Fig.7 (d) shows that there were many holes in the AgO layer even it covered the outer layer of the polarized silver. The electrolyte penetrated through the polarized layer and covered some active sites of the basal silver. The active sites were polarized to be Ag_2O owing to autocatalytic effect of AgO. The second anodic peak 'paA0'was formed during the reversed scan because the scan rate was too big for this autocatalytic process. The secondary anodic peak 'paA1' in Fig. 3 should be the continuous anodic reaction $Ag_2O \rightarrow AgO$ during the continuous cathodic scan.

5. CONCLUSIONS

The effects of electrochemical parameters, such as the numbers of cycle, scan rate and NaOH concentration, on formation and reduction of silver oxides were investigated with CV and images. The shapes of the peaks changed much from the first cycle to the other cycles because of the different surface before and after the first cycle. Pre-peaks and peaks of Ag_2O were contributed to the formation of the dual layers of Ag_2O on silver's surface polarized by CV method in NaOH solution. The peak characteristic was dependent of scan rate and NaOH concentration. The midpoint current density of the peaks increased with increase in scan rate and NaOH concentration. The midpoint potential shifted positive during anodic scan and negative during cathodic scan with increasing scan rate, while shifted reversed with increasing NaOH concentration. Secondary anodic peaks appeared during the reversed scan of the first cycle if the scan rate or NaOH concentration was big enough. The phenomenon was explained by the surface images and roughness of silver at various stages of CVs.

ACKNOWLEDGMENTS

The authors gratefully appreciate the financial support from the National Natural Science Foundation of China (Grant No.: 51101106), the State Key Program of National Natural Science of China (Grant No. 51131007) and Program for Innovative Research Talent by the Ministry of Liaoning Education (Grant No.: LR2012019).

References

1. A.P. Karpinski , S.J. Russell, J.R. Serenyi and J.P. Murphy, *J. Power Sources*, 91 (2000) 77.
2. J.M.M. Droog and F. Huisman, *J. Power Sources*, 115 (1980) 211.
3. T.U. Hur and W.S.Chung, *J. Electrochem. Soc.*, 152 (2005): A996.
4. J. Ambrose and R.G. Barradas, *Electrochim. Acta*, 19 (1974) 781.
5. P. Stonehart, *Electrochim. Acta*, 13 (1968) 1789.
6. M.L. Teijelo, J.R. Vilche and A. J. Arvia, *J. Appl. Electrochem.*, 18 (1988) 691.
7. P. Stonehart and F.P. Portante, *Electrochim. Acta*, 13 (1968) 1805.
8. B.G. Pound, D.D. Macdonald and J.W. Tomlinson, *Electrochim. Acta*, 25 (1980) 563.
9. N. Iwasaki, Y. Sasaki and Y. Nishina, *Surf. Sci.*, 198 (1988) 524.
10. D. Hecht, P. Borthen and H.H. Strehblow, *Surf. Sci.*, 365 (1996) 263.
11. N. Sato and Y. Shimizu, *Electrochim. Acta*, 18 (1973) 567.
12. M. Hepel and M. Tomkiewicz, *J. Electrochem. Soc.*, 133 (1986) 1625.
13. Z. Takehara, Y. Namata and S. Yoshizawa, *Electrochim. Acta*, 13 (1968) 1395.
14. R.D. Giles, J.A. Harrison and H.T. Thirsk, *J. Electroanal. Chem. Interfa. Electrochem.*, 22 (1969) 375.
15. B.V. Tilak, R.S. Perkins, H.A. Kozlowska and B.E. Conway, *Electrochim. Acta*, 17 (1972) 1447.
16. N.A. Hampson, K.J. MacDonald and J. B. Lee. *J. Electroanal. Chem.*, 45 (1973) 149.
17. M. Fleischmann, D.J. Lax and H.R. Thirsk, *Trans. Faraday Soc.*, 64 (1968) 3137.
18. R.S. Perkins, B.V. Tilak, B.E. Conway and H.A. Kozlowska, *Electrochim. Acta*, 17 (1972) 1471.
19. G.W.D. Briggs, M. Fleischmann, D.J. Lax and H.R. Thirsk, *Trans. Faraday Soc.*, 64 (1968) 3120.
20. X. Zhang, S. Stewart, D.W. Shoesmith and J.C. Wren, *J. Electrochem. Soc.*, 154 (2007) F70.
21. Z.Y. Chen, D. Liang, G. Ma, G.S. Frankel, H.C. Allen and R.G. Kelly, *Corros. Eng. Sci. Technol.*, 45 (2010) 169.
22. T.D. Grozdić and L.D. Stojić, *J. Power Sources*, 79 (1999) 1.
23. J.M.M. Droog, P.T. Alderliesten and G.A. Bootsma, *J. Electroanal. Chem. Interfa. Electrochem.*, 99(1979) 173.
24. M.W. Aylward and P.G. Pickup, *Electrochim. Acta*, 52 (2007) 6275.
25. K. Choi and H.H. Kim, *J. Appl. Polym. Sci.*, 44 (1992) 751.
26. S.M. Ebrahim, M.M.A. Latif, A.M. Gad and M.M. Soliman, *Thin Solid Films*, 518 (2010) 4100.
27. K. David and J. Gosser, *Cyclic Voltammetry, Simulation and analysis of reaction mechanisms*, VCH Publishers, UK (1993).
28. A.M. Bond, *Inorg. Chim. Acta*, 226 (1994) 293.
29. Y. Wan, Y.B. Li, Q. Wang, K. Zhang and Y.H. Wu, *Inter. J. Electrochem. Sci.*, 7 (2012) 5204.